INTERNATIONAL JOURNAL FOR NUMERICAL METHODS IN FLUIDS, VOL. 17, 605–633 (1993)

FLOW OF VISCOELASTIC FLUIDS THROUGH A POROUS CHANNEL—I

P. D. ARIEL

Department of Mathematics and Computer Science, Moi University, P.O. Box 3900, Eldoret, Kenya

SUMMARY

The flow of viscoelastic fluids through a porous channel with one impermeable wall is computed. The flow is characterized by a boundary value problem in which the order of the differential equation exceeds the number of boundary conditions. Three solutions are developed: (i) an exact numerical solution, (ii) a perturbation solution for small R, the cross-flow Reynold's number and (iii) an asymptotic solution for large R. The results from exact numerical integration reveal that the solutions for a non-Newtonian fluid are possible only up to a critical value of the viscoelastic fluid parameter, which decreases with an increase in R. It is further demonstrated that the perturbation solution gives acceptable results only if the viscoelastic fluid parameter is also small.

Two more related problems are considered: fluid dynamics of a long porous slider, and injection of fluid through one side of a long vertical porous channel. For both the problems, exact numerical and other solutions are derived and appropriate conclusions drawn.

KEY WORDS Viscoelastic fluids Finite differences Shooting method Flow through a channel Porous slider Flow through a vertical wall

1. INTRODUCTION

The study of flow of viscoelastic fluids has aroused considerable interest and controversy since Beard and Walters[1] first considered the two-dimensional flow near a stagnation point. The focus of interest centred around the fact that the constitutive equations of viscoelastic fluids give rise to a Boundary Value Problem (BVP) in which the order of differential equation exceeds the number of boundary conditions. Thus, for the two-dimensional stagnation point flow the BVP characterizing the flow is

$$f'''+ff''+1-f'^2+k(ff^{\text{iv}}-2f'f'''+f''^2)=0, \tag{1}$$

with the boundary conditions

$$f(0)=0, \qquad f'(0)=0, \qquad f'(\infty)=1, \tag{2}$$

where f is the dimensionless stream function, k is the non-dimensional viscoelastic fluid parameter and prime denotes the derivative with respect to η, the similarity variable.

Beard and Walters[1] proposed to resolve the difficulty associated with the higher order of the differential equation in comparison with the number of available boundary conditions by seeking a linear perturbation expansion for f as follows:

$$f=f_0+kf_1, \tag{3}$$

where f_0 is the solution corresponding to the Newtonian fluid and f_1 is the perturbation due to the

0271–2091/93/190605–29$19.50

Received August 1992
Revised April 1993

viscoelasticity of the fluid. It can easily be seen that if equation (1) is expanded up to the first-order term in k, it gives rise to a pair of BVPs in which the order of the highest derivative matches with the number of boundary conditions. The numerical solution of the resulting BVPs can be obtained by any integration routine. Beard and Walters[1] used the Runge–Kutta method to find the solutions for f_0 and f_1.

Since then, numerous other flow problems of viscoelastic fluids have been considered by various investigators.[2–5] In all these investigations similar BVPs resulted, and the same approach as in equation (3) was chosen to solve the BVPs.

The main conclusion of Beard and Walters[1] was that, for a viscoelastic fluid, the velocity in the boundary layer exceeds its value in the mainstream flow. This rather unexpected result naturally led to a controversy. Frater[6] was of the opinion that the conclusion was faulty and its origin lay in the perturbation expansion given by (3). He gave an example demonstrating his point, though the example chosen by him was from a different context. The issue of the velocity overshooting its value in the mainstream, it was felt, could only be resolved by obtaining an accurate numerical solution of BVP (1) and (2). However, for a long time it was thought that any attempt to numerically integrate BVP (1) and (2) was destined to end in a failure, mainly because of the behaviour of the coefficient of f^{iv} in equation (1) near $\eta=0$, which is $O(k\eta^2)$. Serth[7] reported numerical instability when the integration routines such as the Runge–Kutta method or the predictor–corrector methods are tried. He, instead, used the collocation point method with different polynomials. Unfortunately, the number of trial functions in his velocity profile rose sharply with an increase in the value of k. Ng[8] was able to reduce the number of trial functions dramatically by using the technique of goal programming, but then it was not clear as to which choice of collocation points would give the desired result.

It was Teipel[9] who was first successful in obtaining the numerical solution of the BVP (1) and (2). He evolved a shooting method in which a Taylor series expansion was sought for f around $\eta=0$ in terms of $f''(0)$. This was used for developing the solution till $\eta=0{\cdot}1$. For values of $\eta>0{\cdot}1$, the usual Runge–Kutta method was used to obtain the solution. Teipel demonstrated that oscillations take place in the transverse velocity about its value in the mainstream, implying that the conclusions of Beard and Walters[1] were essentially sound. However, he had to exercise great care in supplying accurate initial conditions for the Runge–Kutta method. Thus, he had to find the ninth derivative of equation (1) to ensure the necessary accuracy. This probably explains the failure of early attempts to numerically integrate equation (1). It may be further remarked that Teipel's approach is likely to cause even greater problems when $k\to 0$, i.e. when the fluid is slightly non-Newtonian. The present author,[10] on the other hand, gave an algorithm which is free of the above-mentioned drawbacks. What is particularly pleasing is the fact that the said algorithm is equally applicable for all values of k, including the cases $k=0$ and $k\to 0$. Use of this algorithm revealed that the solutions of BVP (1) and (2) exist only up to a critical value of k, say, k_c, and that there are dual solutions for all non-zero values of k less than k_c. These conclusions cannot possibly be derived by a linear perturbation analysis based on equation (3). This fact naturally has put under cloud the earlier investigations such as those in References[2–5], which were based on the perturbation technique. These problems being important physically need to be re-examined so that the study of flow of viscoelastic fluids may be put in the proper perspective.

In the present paper our main endeavor is to study the flow of a viscoelastic fluid through a flat channel in which one of the boundaries is porous through which the fluid is injected at a uniform rate. The other boundary is assumed to be impermeable. This is a basic problem and, we believe, it provides an insight into the flow of viscoelastic fluids through the porous boundaries. As will be seen later, it also finds application in other technological problems. The flow of viscoelastic fluid through a porous channel was first considered by Shrestha,[2] who assumed both the walls of the channel to be porous with different permeability. He obtained a perturbation solution in the limits of small k, as well as small R, the cross-flow Reynold's number. In the present paper, using a slightly modified version of the algorithm given in Reference 10, an exact numerical solution is obtained without making any assumption on the size of k or R. It is also shown that as far as a perturbation solution for small R is concerned, it is not essential to assume k small simultaneously, in principle at any rate. Finally, utilizing the technique of matched asymptotic expansion, the solution is derived for large values of R. The results are compared using the various techniques.

Recall that for the present problem we have assumed one wall to be impermeable. In the second part of the paper we intend to investigate the case when both the walls are porous, but the rate of injection at both the walls is same. Finally, in the third part of the paper the most general and difficult case of unequal rates of injection of the fluid at the two walls will be treated.

However, in the present paper we have considered two more related problems of flow of viscoelastic fluid: (i) the fluid dynamics of a long porous slider and (ii) injection of fluid through a wall of a long vertical channel. For a Newtonian fluid these problems have been investigated by Skalak and Wang[11] and Wang and Skalak,[12] respectively. The exact numerical results obtained for all the three problems considered in the present work strongly point to the conclusion that *the perturbation technique is not guaranteed to produce the correct results qualitatively or quantitatively, and that, the exact solutions (analytical or numerical) must be sought of the original set of equations, rather than those of the perturbed sets of equations.*

2. CONSTITUTIVE EQUATIONS

In this paper we are mainly concerned with the flow of a particular class of viscoelastic fluids, namely, Walter's B' fluids. For these fluids, also known as elasticoviscous fluids, the constitutive equation is

$$P_{ik} = -pg_{ik} + p'_{ik}, \tag{4}$$

where p_{ik} is the stress tensor, p is the scalar pressure at a point and g_{ik} is the metric tensor of a fixed co-ordinate system x^i. Finally p'_{ik}, in contravariant form, is given by

$$p'^{ik} = 2\eta_0 e^{ik} - 2k_0 \tilde{e}^{ik}. \tag{5}$$

In equation (5), e^{ik} is the rate of strain tensor defined by

$$e^{ik} = \tfrac{1}{2}(v^i_{,k} + v^k_{,i}) \tag{6}$$

and $\tilde{e}^{ik}$ is given by

$$\tilde{e}^{ik} = \frac{\partial e^{ik}}{\partial t} + v^j e^{ik}_{,j} - v^k_{,j} e^{ij} - v^i_{,j} e^{ik}, \tag{7}$$

where v^i is the velocity vector, and a comma denotes differentiation. Finally η_0 and k_0 are, respectively, the limiting viscosity at small rate of shear and the short-memory coefficient, defined by

$$\eta_0 = \int_0^\infty N(\tau)\,\mathrm{d}\tau, \qquad k_0 = \int_0^\infty \tau N(\tau)\,\mathrm{d}\tau. \tag{8}$$

$N(\tau)$ being the distribution function with relaxation time τ.

For Walter's B' fluid with very short memories, the terms involving

$$\int_0^\infty \tau^n N(\tau)\,\mathrm{d}\tau, \quad n \geqslant 2$$

have been neglected. This factor has been taken into consideration in deriving equation (5).

Lastly, the equations of motion and continuity are

$$\rho\left(\frac{\partial v^i}{\partial t}+v^j v^i_{,j}\right)=-p_{,i}+p'^{ij}_{,j} \tag{9}$$

and

$$v^i_{,i}=0, \tag{10}$$

3. FLOW THROUGH A POROUS CHANNEL

In this section we consider the laminar flow of an incompressible Walter's B' fluid through a channel bound by the planes $y=0$, which is impermeable, and $y=d$, which is porous. We take the direction of flow along x-axis. The fluid is injected through the porous wall with uniform velocity V. For the problem under consideration, equations of motion (9) and continuity (10) become

$$\rho\left(u\frac{\partial u}{\partial x}+v\frac{\partial u}{\partial y}\right)=-\frac{\partial p}{\partial x}+\frac{\partial p'_{xx}}{\partial x}+\frac{\partial p'_{xy}}{\partial y}, \tag{11}$$

$$\rho\left(u\frac{\partial v}{\partial x}+v\frac{\partial v}{\partial y}\right)=-\frac{\partial p}{\partial y}+\frac{\partial p'_{yx}}{\partial x}+\frac{\partial p'_{yy}}{\partial y} \tag{12}$$

and

$$\frac{\partial u}{\partial x}+\frac{\partial v}{\partial y}=0, \tag{13}$$

where (u,v) are the components of the velocity vector v^i and $p'_{xx}, p'_{xy}, p'_{yy}$ are the non-vanishing components of p'^{ij}, and are given by

$$p'_{xx}=2\eta_0\frac{\partial u}{\partial x}-2k_0\left[u\frac{\partial^2 u}{\partial x^2}+v\frac{\partial^2 u}{\partial x\partial y}-2\left(\frac{\partial u}{\partial x}\right)^2-\frac{\partial u}{\partial y}\left(\frac{\partial u}{\partial y}+\frac{\partial v}{\partial x}\right)\right]$$

$$p'_{xy}=p'_{yx}=\eta_0\left(\frac{\partial u}{\partial y}+\frac{\partial v}{\partial x}\right)-k_0\left[u\left(\frac{\partial^2 u}{\partial x\partial y}+\frac{\partial^2 v}{\partial x^2}\right)+v\left(\frac{\partial^2 u}{\partial y^2}+\frac{\partial^2 v}{\partial x\partial y}\right)\right.$$
$$\left.+2\left(\frac{\partial u}{\partial x}\frac{\partial u}{\partial y}+\frac{\partial v}{\partial x}\frac{\partial v}{\partial y}\right)\right]$$

$$p'_{yy}=2\eta_0\frac{\partial v}{\partial y}-2k_0\left[u\frac{\partial^2 v}{\partial x\partial y}+v\frac{\partial^2 v}{\partial y^2}-\frac{\partial v}{\partial x}\left(\frac{\partial u}{\partial y}+\frac{\partial v}{\partial x}\right)-2\left(\frac{\partial v}{\partial y}\right)^2\right].$$

The boundary conditions on u and v are

$$\begin{aligned} u(x,0)&=0, \qquad u(x,d)=0\\ v(x,0)&=0, \qquad v(x,d)=-V. \end{aligned} \tag{14}$$

Following the standard practice, we look for similarity solutions of equations (11)–(13) in which the stream function ψ is given by (see, e.g. Reference 13)

$$\psi(x,\eta)=(Vx-U_0 d)f(\eta), \tag{15}$$

where

$$\eta=\frac{y}{d} \tag{16}$$

and U_0 is the entrance velocity defined by

$$U_0=\int_0^1 u(0,\eta)\,\mathrm{d}\eta. \tag{17}$$

The velocity components u and v are then given by

$$u=\frac{\partial\psi}{\partial y}=\left(\frac{Vx}{d}-U_0\right)f'(\eta), \qquad v=-\frac{\partial\psi}{\partial x}=-Vf(\eta), \tag{18}$$

where a prime denotes a derivative with respect to η.

Substituting for u and v from equation (18) into equations (11) and (12), we obtain

$$\frac{\partial p}{\partial x}=\frac{\eta_0}{d^2}\left(\frac{Vx}{d}-U_0\right)[f'''+R(ff''-f'^2)+Rk(ff^{\mathrm{iv}}-2f'f'''+f''^2)] \tag{19}$$

$$\frac{\partial p}{\partial \eta}=-\frac{V\eta_0}{d}[f''-Rff'+Rk(ff'''-3f'f'')], \tag{20}$$

where

$$R=\frac{\rho Vd}{\eta_0} \tag{21}$$

and

$$k=\frac{k_0}{\rho d^2} \tag{22}$$

are cross-flow Reynold's number and dimensionless measure of viscoelasticity of the fluid, respectively.

Integrating equation (20) with respect to η, we get

$$p=-\frac{V\eta_0}{d}[f'-\tfrac{1}{2}Rf^2+Rk(ff''-2f'^2)]+P(x), \tag{23}$$

where $P(x)$ is an arbitrary function of x.

Differentiation of (23) with respect to x yields

$$\frac{\partial p}{\partial x}=P'(x). \tag{24}$$

Combining equations (19) and (24), we obtain

$$P'(x)=\frac{\eta_0}{d^2}\left(\frac{Vx}{d}-U_0\right)[f'''+R(ff''-f'^2)+Rk(ff^{\mathrm{iv}}-2f'f'''+f''^2)] \tag{25}$$

It is clear that the quantity inside the brackets in equation (25) must be independent of η and, therefore, a constant, say A. Hence, we have the following BVP for f:

$$f'''+R(ff''-f'^2)+Rk(ff^{\mathrm{iv}}-2f'f'''+f''^2)=A, \tag{26}$$

with the boundary conditions

$$f(0)=0, \qquad f'(0)=0, \qquad f(1)=1, \qquad f'(1)=0, \tag{27}$$

which can be obtained by combining equations (14) and (18).

It may be remarked here that for a second-order fluid, f satisfies an identical BVP, with $k=-K$, K, being the viscoelastic fluid parameter.

Using equation (26), $P'(x)$ can now be written as

$$P'(x)=\frac{A\eta_0}{d^2}\left(\frac{Vx}{d}-U_0\right)$$

which, when integrated, gives

$$P(x)=p_0+\frac{A\eta_0 x}{d^2}\left(\frac{Vx}{2d}-U_0\right), \tag{28}$$

where p_0 is the constant of integration.

Inserting $P(x)$ from equation (28) into equation (23), we get the following expression for pressure:

$$p(x,\eta)=p_0+\frac{A\eta_0 x}{d^2}\left(\frac{Vx}{2d}-U_0\right)-\frac{V\eta_0}{d}\left[f'-\tfrac{1}{2}Rf^2+Rk(ff''-2f'^2)\right], \tag{29}$$

It is easy to see that the constant p_0 is, in fact, the pressure at (0, 0). Thus, if one can solve the BVP (26) and (27) for f, the flow is completely determined from equations (18) which express the velocity distribution in terms of f, and equation (29), which gives the pressure at a point. In the next few sections, we give various solutions for f.

3.1. Exact numerical solution for arbitrary R

When $k=0$, i.e. for a Newtonian fluid, equation (26) is a third-order differential equation. There are four boundary conditions on f given by equation (27). However, there is an unknown constant A in equation (26), which may, therefore, be regarded as the eigenvalue of the BVP (26) and (27). When $k\neq 0$, i.e. for a non-Newtonian fluid, equation (26) becomes a fourth-order differential equation, *plus* there is the unknown constant A. There are still only four boundary conditions of f. Hence, we have a situation similar to the one corresponding to the two-dimensional stagnation point flow characterized by BVP (1) and (2). We can, therefore, apply the same numerical technique as given by the present author.[10]

Let us then introduce the quantities y as under

$$y_1=f, \qquad y_2=f', \qquad y_3=f'', \tag{30}$$

whence the BVP (26) and (27) can be rewritten as

$$y_3'+R(y_1y_3-y_2^2)+Rk(y_1y_3''-2y_2y_3'+y_3^2)=A, \tag{31}$$

with the boundary conditions

$$y_1(0)=0, \qquad y_2(0)=0, \qquad y_1(1)=1, \qquad y_2(1)=0. \tag{32}$$

For the purpose of discretization, we set up a mesh

$$\eta_i=ih \quad (i=0,1,\ldots,N), \tag{33}$$

where N is a suitable integer, and $h(=1/N)$ is the mesh-size.

For the derivatives of y_3 occuring in equation (31), we use the central difference formulae

$$F'(\eta_i)=\frac{F^{i+1}-F^{i-1}}{2h}, \qquad F''(\eta_i)=\frac{F^{i+1}-2F^i+F^{i-1}}{h^2}, \tag{34}$$

with an error $O(h^2)$.

Hence, equation (31) can be discretized to

$$\frac{y_3^{j+1}-y_3^{j-1}}{2h}+R[y_1^j y_3^j-(y_2^j)^2]+Rk\left[y_1^j\frac{y_3^{j+1}-2y_3^j+y_3^{j-1}}{h^2}-2y_2^j\frac{y_3^{j+1}-y_3^{j-1}}{2h}+(y_3^j)^2\right]=A, \quad (35)$$

which can be explicitly solved for y_3^{j+1} to yield

$$y_3^{j+1}=\left[1+2Rk\left(\frac{y_1^j}{h}-y_2^j\right)\right]^{-1}\left\{\left[1-2Rk\left(\frac{y_1^j}{h}+y_2^j\right)\right]y_3^{j-1}\right.$$
$$\left.-2hRy_3^j\left[y_1^j-k\left(\frac{2y_1^j}{h^2}-y_3^j\right)\right]+2h[A+R(y_2^j)^2]\right\}, \quad (36)$$

with a truncation error $O(h^3)$.

y_2^{j+1} and y_1^{j+1} can be obtained by discretizing the relations

$$y_2'=y_3, \qquad y_1'=y_2, \quad (37)$$

using the approximations

$$y_2^{j+1}=y_2^j+\tfrac{1}{2}h(y_3^j+y_3^{j+1}), \quad (38)$$

$$y_1^{j+1}=y_1^j+\tfrac{1}{2}h(y_2^j+y_2^{j+1}) \quad (39)$$

the error in equations (38) and (39) being $O(h^3)$.

The boundary conditions (32) get transformed to

$$y_1^0=0, \qquad y_2^0=0, \qquad y_1^N=1, \qquad y_2^N=0. \quad (40)$$

Note that in equation (36), the values of y_3 are at three adjacent mesh points $j-1, j$ and $j+1$. If y_3^0 is known, then in order to start the recursion, one also needs to know the value of y_3^1. This value can be obtained conveniently by seeking a Taylor series expansion of f'' around $\eta=0$. We have

$$y_3^1=f''(h)=f''(0)+hf'''(0)+\frac{h^2}{2!}f^{\text{iv}}(0)+O(h^3)$$
$$=f''(0)+h(A-Rk[f''(0)]^2). \quad (41)$$

It can be easily verified by differentiating equation (26) that $f^{\text{iv}}(0)=0$.

Let

$$f''(0)=s.$$

Assuming s and A are known, y_3^1 can be obtained from equation (41). y_2^1 and y_1^1 can then be found from equations (38) and (39) on making use of boundary conditions (40). From this point on, y_3^j can be determined from equation (36) for $j \geq 2$. Thus, we obtain y_3^2 from equation (36), then y_2^2 from equation (38) and finally y_1^2 from equation (39). The cycle is repeated till y's are computed at all the mesh-points. Thus, we see that the problem reduces to the determination of the appropriate values of the quantities s and A such that the terminal conditions in equation (40) are satisfied. For this any zero-finding algorithm can be used. Two of the commonly used algorithms suggest themselves, namely, secant method and the generalized Newton's method. For the latter, one set of trial values suffices, but then at each iteration, the values of $\partial y/\partial s$ and $\partial y/\partial A$ are also required. This roughly triples the size of the problem. On the other hand, for the secant method three sets of trial values are required to start the iteration, however, after this only one set of values of s and A is needed at each iteration. The starting values can be chosen as the same for the generalized Newton's method and a pair of slightly perturbed values. Though the convergence of the Newton's method is quadratic, there is still a substantial saving of CPU time using the secant method. We have, therefore, chosen it to compute the missing values of $f''(0)$ and A.

The solution for f (and its derivatives), of course, depends on the choice of the physical parameters R and k. For $k=0$, the solution can be obtained by one of the standard techniques such as shooting method, quasi-linearization, finite differences, etc. It seems natural, for a given value of R, to obtain the solution first for $k=0$, and then to increase the value of k systematically. For non-zero values of k, the solution was obtained by using the algorithm outlined above. As a matter of fact, the algorithm can also be used with equal ease for $k=0$, at least for up to moderate values of R. Several values of R were chosen. For each of these values, k was increased from zero and corresponding values of s and A determined iteratively, along with the desired values of f and f'. No difficulties were encountered to begin with as only 6–7 iterations were sufficient to produce an accuracy of eight significant digits in the values of s and A. However, for values of k exceeding some critical value k_c no convergence could be attained. Thus, we have a situation similar to one encountered in two-dimensional stagnation point flow of a viscoelastic fluid,[10] and this was true for all values of R, the cross-flow Reynold's number. Anticipating the presence of turning points in the solution, once again the roles of s and k were reversed, i.e. rather than getting the values of s and A for given values of R and k, the values of k and A were determined for given values of R and s. The value of s was increased from the value of $f''(0)$ when $k=0$ for a given R, and the corresponding values of k and A were calculated. The results are presented in Figure 1 in which $f''(0)$ is plotted against k for several values of R. One can note that, for each value of R, there is a turning point at $k=k_c$ which is dependent on R. For $k>k_c$ no

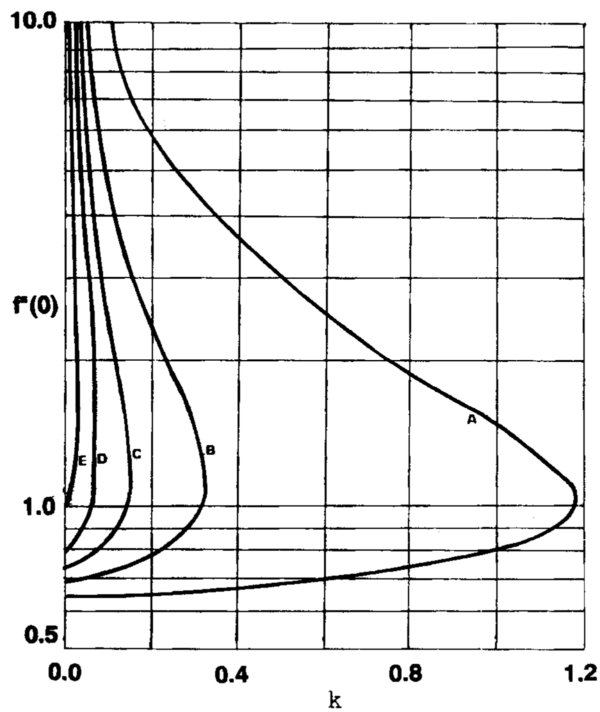

Figure 1. Flow through a porous channel—variation of $f''(0)$ with k, the viscoelastic parameter for various values of R, the cross-flow Reynold's number. Curve A: $R=1$, Curve B: $R=2$, Curve C: $R=3$, Curve D: $R=5$, Curve E: $R=10$

solution exists, while for $0<k<k_c$ dual solutions exist. This conclusion, it can be seen, is in line with the one reported for the stagnation point flow.[10]

The dependence of k_c on R is quite important. From Figure 1 it is clear that as R is increased, the value of k_c decreases. In Figure 2, k_c is plotted against R on a logarithmic scale. It is most instructive to find that for large values of R, the value of Rk_c becomes stationary. This fact has a vital bearing on the asymptotic solution for large values of R, which is presented in a later section.

A slight modification is necessary in the implementation of the above algorithm for large values of $R(>70)$. For these values, the shooting method becomes very sensitive to the trial values of s and A: a slight perturbation in these values causing large changes in the values of y_1^N and y_2^N, sometimes to the extent of resulting into machine overflow. This problem of numerical instability is not only apparent when $k\neq 0$, but is also present when $k=0$. It was resolved by replacing the value of y_3 in the second term of equation (31) by the average at the adjacent nodes. Thus, for large values of R, equation (35) gets modified to

$$\frac{y_3^{j+1}-y_3^{j-1}}{2h}+R[\tfrac{1}{2}y_1^j(y_3^{j+1}+y_3^{j-1})-(y_2^j)^2]$$
$$+Rk\left[y_1^j\frac{y_3^{j+1}-2y_3^j+y_3^{j-1}}{h^2}-2y_2^j\frac{y_3^{j+1}-y_3^{j-1}}{2h}+(y_3^j)^2\right]=A. \tag{42}$$

Note that equation (42) has the same order of truncation error as equation (35). In fact, it can be used for all values of R. Solving equation (42) for y_3^{j+1}, we get

$$y_3^{j+1}=\left[1+hRy_1^j+2Rk\left(\frac{y_1^j}{h}-y_2^j\right)\right]^{-1}\left\{\left[1-hRy_1^j-2Rk\left(\frac{y_1^j}{h}+y_2^j\right)\right]y_3^{j-1}\right.$$
$$\left.+2hRky_3^j\left(\frac{2y_1^j}{h^2}-y_3^j\right)+2h[A+R(y_2^j)^2]\right\}. \tag{43}$$

When equation (43) was used in place of equation (36), no difficulties were encountered for values of R up to 100. The higher values of R were not attempted. However, with a proper choice of the mesh-size h, we do not anticipate any difficulty for these values of R.

3.2. *Perturbation solution for small R*

In this section we present the solution for small cross-flow Reynolds number. These solutions have been extensively obtained in the literature and it would be of interest to find out how they compare with the exact numerical solution. In particular, one would be interested in knowing the range of values of R and k for which these solutions would give acceptable results.

Expanding f and A in the form

$$f=f_0+Rf_1+R^2f_2+\cdots,$$
$$A=A_0+RA_1+R^2A_2+\cdots, \tag{44}$$

the BVPs for f_i are

$$f_0'''=A_0,$$
$$f_0(0)=0, \qquad f_0'(0)=0, \qquad f_0(1)=1, \qquad f_0'(1)=0 \tag{45}$$

and

$$f_i''' + \sum_{j=0}^{i-1} [f_{i-1}f''_{i-1-j} - f'_{i-1}f'_{i-1-j} + k(f_{i-1}f^{\text{iv}}_{i-1-j} - 2f'_{i-1}f'''_{i-1-j} + f''_{i-1}f''_{i-1-j})] = A_i$$
$$f_i(0)=0, \quad f'_i(0)=0, \quad f_i(1)=0, \quad f'_i(1)=0, \quad i=1,2,\cdots. \tag{46}$$

The solutions of BVPs (45) and (46) are straightforward. We list below the resulting solutions for f and A up to terms of R^2:

$$\begin{aligned} f(\eta) = {} & 3\eta^2 - 2\eta^3 + R\left(\frac{8}{35}\eta^2 - \frac{27}{70}\eta^3 + \frac{3}{10}\eta^5 - \frac{1}{5}\eta^6 + \frac{2}{35}\eta^7\right) \\ & + R^2\left[-\frac{761}{646\,800}\eta^2 - \frac{2929}{323\,400}\eta^3 + \frac{8}{175}\eta^5 - \frac{113}{2100}\eta^6\right. \\ & + \frac{27}{1225}\eta^7 - \frac{3}{560}\eta^8 + \frac{1}{210}\eta^9 - \frac{2}{525}\eta^{10} + \frac{4}{5775}\eta^{11} \\ & \left. + k\left(\frac{3}{14}\eta^2 - \frac{12}{35}\eta^3 + \frac{3}{10}\eta^6 - \frac{6}{35}\eta^7\right)\right] + O(R^3), \end{aligned} \tag{47}$$

$$A = -\left[12 + \left(\frac{81}{35} - 36k\right)R + \left(\frac{2929}{53\,900} - \frac{24}{7}k\right)R^2\right] + O(R^3). \tag{48}$$

It may be remarked here that Shrestha[2] first expanded f into f_0 and f_1 (see equation (3)) in order to derive the perturbation solution for small R. He then obtained solution for both f_0 and f_1 for small R. As can be seen above, it should not be necessary, although the final expression obtained by Shrestha is in agreement with the one given in equation (47).

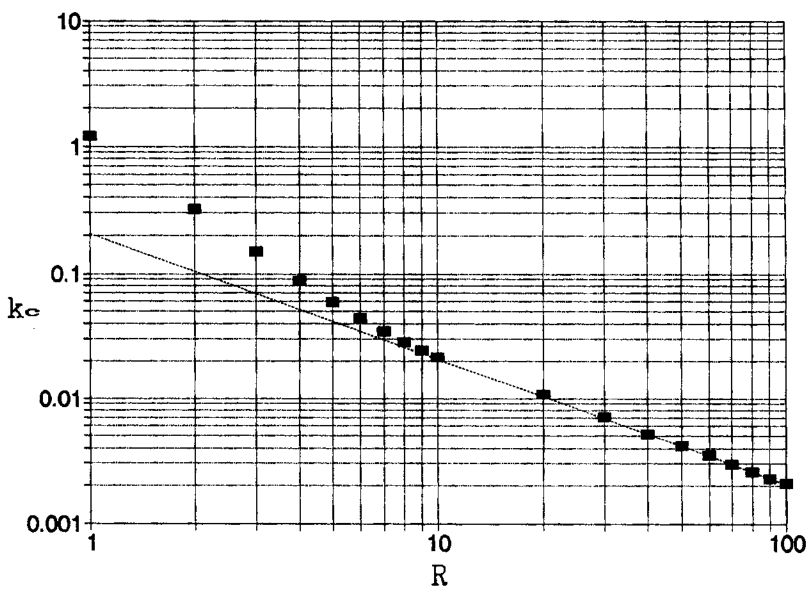

Figure 2. Flow through a porous channel—variation of k_c, the critical value of the viscoelastic parameter k, with R, the cross-flow Reynold's number. (■): the exact value of k_c; (-----): the asymptotic value of k_c for large R and satisfies $k_c R = \gamma$, where γ is given by equation (62)

3.3. Asymptotic solution for large R

The key point in deriving the asymptotic solution of f for large R is the realization that as $R \to \infty$, Rk remains bounded for admissible solutions. Letting

$$Rk=\alpha, \tag{49}$$

equation (26) can be restated as

$$f'''+R(ff''-f'^2)+\alpha(ff^{\mathrm{iv}}-2f'f'''+f''^2)=A. \tag{50}$$

For outer solution we write

$$f=f_0+\varepsilon f_1+\varepsilon^2 f_2+\cdots, \tag{51}$$

where

$$\varepsilon=R^{-1/2}. \tag{52}$$

Also let

$$A=A_{-2}\varepsilon^{-2}+A_{-1}\varepsilon^{-1}+A_0+\cdots. \tag{53}$$

The leading terms in the outer expansion are

$$f_0 f_0''-f_0'^2=A_{-2}, \tag{54}$$

$$f_0 f_1''+f_1 f_0''-2f_0' f_1'=A_{-1}. \tag{55}$$

It is apparent that the first two terms of the outer expansion are independent of the non-Newtonian fluid parameter. The solution of equation (54) is

$$f_0=\sin\frac{\pi\eta}{2}, \qquad A_{-2}=-\frac{\pi^2}{4}. \tag{56}$$

It was first given by Proudman.[14]

Substituting for f_0 in equation (55) and using the boundary conditions at $\eta=1$, namely, $f_1(1)=0, f_1'(1)=0$, we obtain

$$f_1=\frac{A_{-1}}{\pi}(1-\eta)\cos\frac{\pi\eta}{2} \tag{57}$$

The constant A_{-1} will be determined by matching the two solutions.

For the inner solution, we stretch both η and f as under

$$\eta=\varepsilon\sqrt{\frac{2}{\pi}}\,Y, \qquad f(\eta)=\varepsilon\sqrt{\frac{\pi}{2}}\,F(Y). \tag{58}$$

Writing

$$F=F_0+\varepsilon F_1+\varepsilon^2 F_2+\cdots \tag{59}$$

the BVP for F_0 is

$$F_0'''+F_0F_0''+1-F_0'^2+\tfrac{1}{2}\pi\alpha(F_0F_0^{\mathrm{iv}}-2F_0'F_0'''+F_0''^2)=0, \tag{60}$$

$$F_0(0)=0, \qquad F_0'(0)=0. \qquad F_0'(\infty)=1. \tag{61}$$

It can be recognized as the one which characterizes the Hiemenz flow[15] for a viscoelastic fluid with $k=(1/2)\,\pi\alpha$. Its solution has been detailed by the present author,[10] who has shown that the solutions are feasible only up to a critical value of the non-Newtonian fluid parameter. In particular, for the BVP (60) and (61) solutions exist for

$$\tfrac{1}{2}\,\pi\alpha<0{\cdot}3257864$$

or

$$Rk<\gamma,\ \text{where}\ \gamma=0{\cdot}2074020. \tag{62}$$

No solutions exist for values of Rk exceeding γ. This relationship between the problems of two-dimensional stagnation point flow and the flow through porous channel is instructive. It explains the non-admissibility of the solutions to the latter problem for values of the viscoelastic fluid parameter beyond a critical value. One may further verify from Figure 2 that the asymptotic value of Rk_c approaches the value of γ given in (62) as $R\to\infty$.

For large Y, the solution of BVP (60) and (61) is

$$F_0=Y+C,\quad Y\to\infty, \tag{63}$$

where C is a constant depending on α. For some selected values of α, C and $F_0''(0)$ are given in Table I.

Matching of the outer solution up to the term of $O(\varepsilon)$ and the leading term of the inner solution gives

$$A_{-1}=C\sqrt{\frac{\pi^3}{2}} \tag{64}$$

The BVP for F_1, the next term in the inner solution for F in equation (59) is

$$F_1'''+F_0F_1''-2F_0'F_1'+F_0''F_1+\tfrac{1}{2}\pi\alpha(F_0F_1^{\text{iv}}-2F_0'F_1''' + 2F_0''F_1''-2F_0'''F_1'+F_0^{\text{iv}}F_1)=2(2/\pi)^{1/2}C \tag{65}$$

$$F_1(0)=0,\qquad F_1'(0)=0,\qquad F_1'(\infty)=-(2/\pi)^{1/2}C. \tag{66}$$

Note that the above BVP has the same characteristic as the BVP (1) and (2), namely that the order of the differential equation exceeds the number of boundary conditions. Nevertheless, it is linear, therefore its solution can be obtained non-iteratively as follows.

Table I. Variation of $F_0''(0)$, C and $F_1''(0)$ with α

α	$F_0''(0)$	C	$F_1''(0)$
0·00	1·232588	−0·647900	0·955779
0·02	1·270308	−0·621376	0·961618
0·04	1·312459	−0·593340	0·967994
0·06	1·360107	−0·563560	0·975126
0·08	1·414750	−0·531630	0·983186
0·10	1·478595	−0·496960	0·992340
0·12	1·555092	−0·458623	1·003056
0·14	1·650111	−0·415052	1·015482
0·16	1·775009	−0·363219	1·029816
0·18	1·957224	−0·295834	1·044227
0·20	2·312115	−0·182645	1·028317

We write

$$F_1 = G + \beta H, \tag{67}$$

where G and H satisfy the initial value problems (IVPs)

$$G''' + F_0 G'' - 2F_0' G' + F_0'' G + \tfrac{1}{2}\pi\alpha(F_0 G^{\text{iv}} - 2F_0' G''' + 2F_0'' G'' - 2F_0''' G' + F_0^{\text{iv}} G) = 2(2/\pi)^{1/2} C, \tag{68}$$

$$G(0)=0, \qquad G'(0)=0, \qquad G''(0)=0$$

and

$$H''' + F_0 H'' - 2F_0' H' + F_0'' H + \tfrac{1}{2}\pi\alpha(F_0 H^{\text{iv}} - 2F_0' H''' + 2F_0'' H'' - 2F_0''' H' + F_0^{\text{iv}} H) = 0, \tag{69}$$

$$H(0)=0, \qquad H'(0)=0, \qquad H''(0)=1.$$

It is easy to see that β can be identified with $F_1''(0)$. It can be determined from the terminal condition and is given by

$$\beta = -\left[\sqrt{\frac{\pi}{2}}\, C + G'(\infty)\right] \Big/ H'(\infty). \tag{70}$$

The IVPs (68) and (69) can be integrated numerically by following the procedure given in Section 3.1 of Reference 10. β can then be calculated from equation (70). Finally, F_1 can be obtained from equation (67). In Figure 3, the plots of F_1 and F_1' are given for various values of α. Also in Table I, the values of $F_1''(0)$ are presented. It can be seen from Figure 3 that F_1 shares many properties with F_0. For example, as k increases $F_1''(0)$ also increases, except near $\alpha = 0{\cdot}2$, where there is a turning point in the solution for F'.[10] Also, in the profiles of F_1', there are

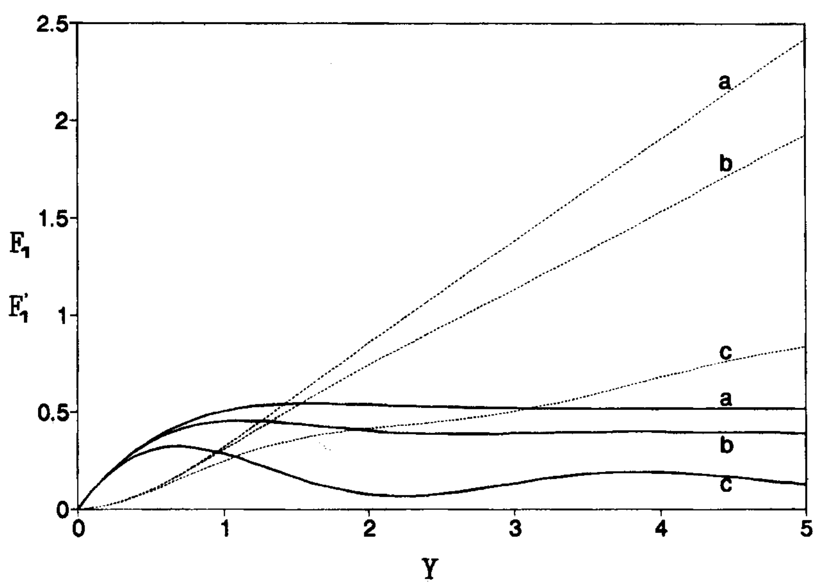

Figure 3. Flow through a porous channel—variation of F_1 and F_1', the first-order terms in the asymptotic expansion of f and f', respectively, with Y for various values of α ($=Rk$). (—): the values of F_1'; (-----): the values of F_1. Curves a: $\alpha=0$, Curves b: $\alpha=0{\cdot}1$, Curves c: $\alpha=0{\cdot}2$

oscillations of increasing amplitude as k is increased. The main difference, of course, is in the asymptotic value of F'_1 as $Y \to \infty$. For F'_0 this limit is always unity; however, for F'_1, because of the decreasing value of $-C$ with k, it approaches smaller asymptotic value as k is increased.

The asymptotic solution of F_1 for large Y is

$$F_1 = -\sqrt{\frac{2}{\pi}}\,CY + D, \quad Y \to \infty, \tag{71}$$

where D is an appropriate constant dependent on α.

The composite solution, which is uniformly valid, can now be written by combining the two solutions. We have

$$f(\eta) = \sin\frac{\pi\eta}{2} + \varepsilon\sqrt{\frac{\pi}{2}}\left[C(1-\eta)\cos\frac{\pi\eta}{2} + F_0(Y) - Y - C\right] + O(\varepsilon^2). \tag{72}$$

F_1 enters in the expression for $f'(\eta)$ as follows:

$$f'(\eta) = \frac{\pi}{2}\left[\cos\frac{\pi\eta}{2} + F'_0(Y) - 1\right] + \varepsilon\sqrt{\frac{\pi}{2}}\left\{-C\left[\cos\frac{\pi\eta}{2} + \frac{\pi}{2}(1-\eta)\sin\frac{\pi\eta}{2}\right]\right.$$
$$\left. + \sqrt{\frac{\pi}{2}}\,F'_1(Y) + C\right\} + O(\varepsilon^2). \tag{73}$$

Thus, the expressions for both u and v (given by equation (18)) are obtained correctly up to $O(\varepsilon^2)$. Undoubtedly, the process of matched asymptotic expansion can further be carried out, but it becomes increasingly complicated. We shall not be pursuing it beyond the terms of $O(\varepsilon)$.

3.4. Results and discussion

In Figures 4 and 5, f and f' are plotted against η for various values of R and k. Three typical values of R are chosen in these figures: 1, 10, 100. They correspond to small, moderate and large values, respectively. Further, keeping in view the restriction (62), three values are chosen for $\alpha\,(=Rk)$: 0, 0·1 and 0·2. One can see that for small values of R, the cross-flow Reynold's number, both f and f' remain relatively unaffected by viscoelasticity of the fluid. Its effect on the flow is felt more for large values of R. In general, an increase in either the value of R or k leads to an increase in f, the transverse velocity. The plots of f', on the other hand, show an increase in f' with increasing R or k near the impermeable wall, but a decrease near the porous wall. Of particular interest is the fact that for a viscoelastic fluid, f' exhibits an oscillatory character if the values of the cross-flow Reynold's number are sufficiently large. This is not surprising and it follows from the asymptotic behaviour of the inner solution near the impermeable wall (see equation (73)).

In Table II, a comparison is presented of the values of $f''(0)$ and $f'''(0)$ obtained by (i) exact numerical integration, (ii) perturbation solution for small R and (iii) asymptotic solution for large R, for various values of R and k. It can be seen from the table that the perturbation solution for small R gives reasonable results for value of cross-flow Reynolds number up to unity *provided* the value of the non-Newtonian fluid parameter is also small (up to 0·2). For moderate values of the non-Newtonian fluid parameter (say, unity), there is a considerable discrepancy in the exact numerical solution and the perturbation solution for small R.

It has been shown that for a viscoelastic fluid, the results, for a given R, can be obtained only up to a critical value of k $(=k_c)$. This sheds new light on the earlier investigation undertaken by Shrestha,[2] who has given, for $k=0{\cdot}2$, the values of $f''(0)$ for the values of R up to 4. It appears that in view of Terrill and Shrestha[16] having demonstrated the perturbation solution (47) to be

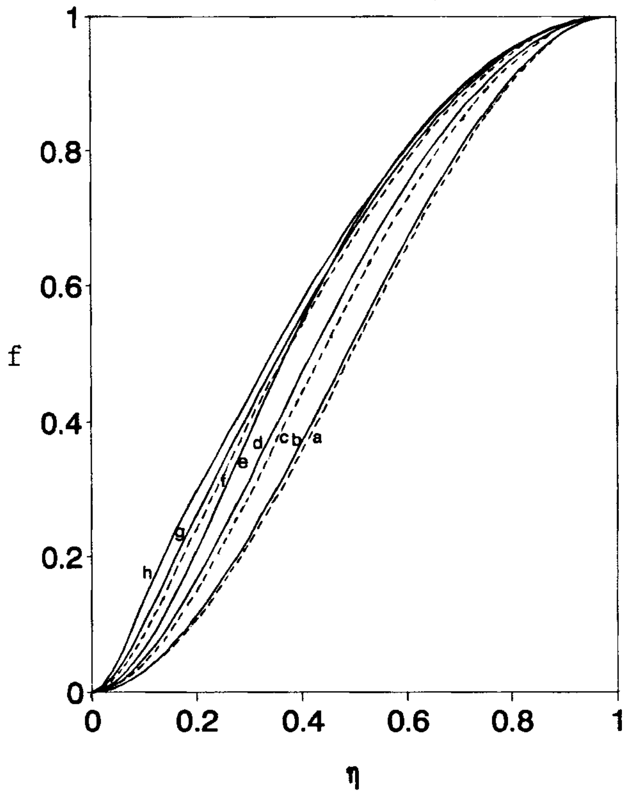

Figure 4. Flow through a porous channel—variation of f, the transverse velocity with η for various values of R, the cross-flow Reynold's number, and k, the viscoelastic parameter. (—): the values of f for a non-Newtonian fluid; (-----): the values for a Newtonian fluid. Curve a: $R=1$, $k=0$; Curve b: $R=1$, $k=0{\cdot}2$; Curve c: $R=10$, $k=0$; Curve d: $R=10$, $k=0{\cdot}01$; Curve e: $=10$, $k=0{\cdot}2$; curve f: $R=100$, $k=0$; Curve g: $R=100$, $k=0{\cdot}001$; Curve h: $R=100$, $k=0{\cdot}002$

reasonably accurate for values of R up to 9 for a Newtonian fluid. Shrestha[2] presumed the same for viscoelastic fluids as well. The present work, however, demonstrates that this assumption is not justified, as for $k=0{\cdot}2$, the solution is admissible for values of R up to 2·56 only.

On the other hand, for large values of R, it can be seen from Table II that the asymptotic solutions (72) and (73) can be used if R is greater than 20–30, *provided* $Rk<\gamma$. For larger values of k, of course, the solution does not exist. It may be added here that for Newtonian fluids the asymptotic results for large R given in Table II are more accurate than those reported by Skalak and Wang,[11] since we have also included the term of F_1 in our calculations.

For the problem at hand, the physical quantities of interest are the stresses at the wall of the channel, which are expressed in terms of $f''(0)$ and $f''(1)$, and the pressure drop along the channel. The values of the former are given in Table II. The latter, in the non-dimensional form, is given by

$$P_x=\frac{p(0,\eta)-p(x,\eta)}{(1/2)\rho U_0^2}=\frac{AR\xi}{Re^2}\left(\frac{2Re}{R}-\xi\right), \tag{74}$$

where

$$\xi=\frac{x}{d} \quad \text{and} \quad Re=\frac{\rho U_0 d}{\eta_0}$$

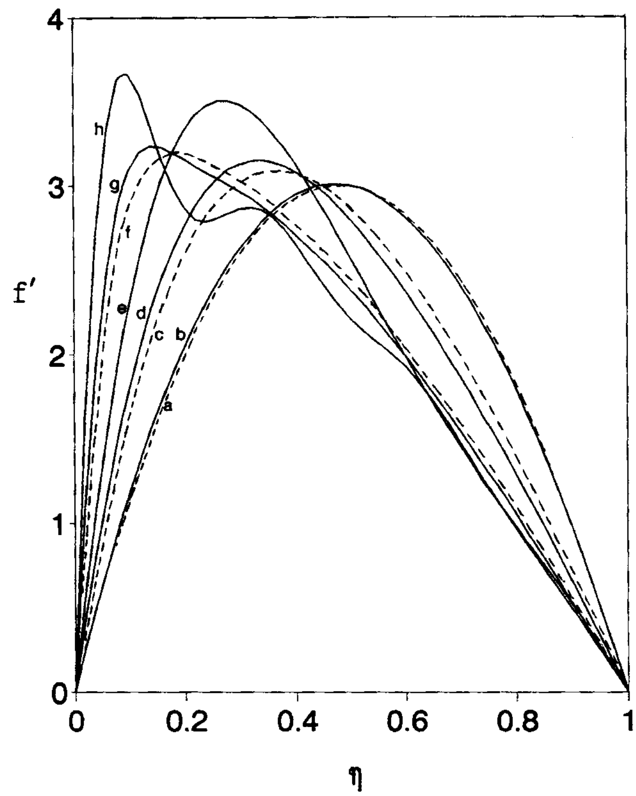

Figure 5. Flow through a porous channel—variation of f', the lateral velocity with η for various values of R, the cross-flow Reynold's number, and k, the viscoelastic parameter. (—): the values of f for a non-Newtonian fluid; (-----): the values for a Newtonian fluid. Curve a: $R=1$, $k=0$; Curve b: $R=1$, $k=0{\cdot}2$; Curve c: $R=10$, $k=0$; Curve d: $R=10$, $k=0{\cdot}01$; Curve e: $R=10$, $k=0{\cdot}02$; Curve f: $R=100$, $k=0$; Curve g: $R=100$, $k=0{\cdot}001$; Curve h: $R=100$, $k=0{\cdot}002$

are, respectively, the non-dimensional distance along the channel and the mainstream Reynold's number.

Keeping R, Re and ξ fixed, it is evident from equation (74) that the pressure drop is proportional to A. Hence, as the viscoelasticity of the fluid increases, the pressure drop decreases.

4. FLUID DYNAMICS OF A LONG POROUS SLIDER

In the present section we consider a long porous slider using the viscoelastic fluid. Porous sliders are becoming increasingly important due to their attractive performance and their application in fluid-cushioned moving pads.[17] The fluid dynamics of a long porous slider using Newtonian fluid has been studied by Skalak and Wang.[11] For other shapes of sliders, Wang and his co-workers have contributed a sequence of papers.[18-21]

We consider a long porous slider of dimensions L_1 and L_2. The fluid is injected through the slider so that a film of thickness d is formed. The lower plate of the slider is moving laterally in the plane $z=0$ with velocities $-U$ and $-V$ along x- and y-directions, respectively. It will further be assumed that $L_2 \gg L_1 \gg d$, so that the end-effects can be neglected.

Table II. Variation of $f''(0), f'''(0)$ and $f''(1)$ with R and k using (i) exact numerical integration, (ii) perturbation solution for small R, and (iii) asymptotic solution for large R

R	k	$f''(0)$		$f'''(0)$		$f''(1)$	
		Exact	Perturbation	Exact	Perturbation	Exact	Perturbation
0·2	0	6·091330	6·091334	−12·465008	−12·465031	−5·893595	−5·893620
	0·1	6·093218	6·093049	−12·473984	−12·473259	−5·892498	−5·892934
	0·2	6·095284	6·094763	−12·483613	−12·481488	−5·890913	−5·892249
	0·5	6·102339	6·099906	−12·515686	−12·506174	−5·883843	−5·890192
	1·0	6·116205	6·108477	−12·577041	−12·547317	−5·866618	−5·886763
1	0	6·454264	6·454790	−14·365856	−14·368627	−5·508899	−5·511933
	0·1	6·518076	6·497647	−14·667341	−14·574341	−5·452446	−5·494790
	0·2	6·601881	6·540504	−15·050191	−14·780056	−5·355036	−5·477647
	0·5	6·957944	6·669075	−16·644702	−15·397199	−4·879748	−5·426218
2	0	6·900850	6·904873	−16·823500	−16·845937	−5·109615	−5·133445
	0·1	7·259711	7·076302	−18·554860	−17·668794	−4·766846	−5·064873
	0·2	7·928913	7·247730	−18·491651	−21·711393	−3·990850	−4·996302

R	k	$f''(0)$		$f'''(0)$		$f''(1)$	
		Exact	Asymptotic	Exact	Asymptotic	Exact	Asymptotic
20	0	13·003861	13·181730	−65·348638	−63·288380	−3·241769	−3·037832
	0·005	14·913310	15·315375	−82·213544	−82·977215	−3·070231	−2·904939
	0·01	20·870849	22·507298	−139·631042	−155·391145	−3·017448	−2·628207
25	0	14·241965	14·415343	−78·860850	−80·518736	−3·138901	−2·977610
	0·004	16·450260	16·815662	−100·321328	−101·059483	−2·982095	−2·858747
	0·008	22·894799	24·896730	−168·779490	−190·809152	−2·705646	−2·611230
50	0	19·179153	19·323624	−145·450549	−144·443440	−2·905645	−2·828173
	0·002	22·493698	22·754334	−189·410066	−190·839906	−2·802498	−2·744124
	0·004	33·484998	34·290862	−352·056742	−365·299273	−2·832337	−2·568104
100	0	26·236914	26·347970	−276·062648	−275·525268	−2·759865	−2·797785
	0·001	31·040678	31·216542	−364·158252	−365·830572	−2·693216	−2·663074
	0·002	46·981957	47·599567	−693·982367	−708·815537	−2·733140	−2·539316

Skalak and Wang[11] have shown that the Navier–Stokes equation for Newtonian fluid admit a similarity solution if the velocity components (u, v, w) are so chosen that

$$u = Ug(\eta) + \frac{Wx}{d} f'(\eta), \qquad v = Vh(\eta), \qquad w = -Wf(\eta), \tag{75}$$

where

$$\eta = \frac{z}{d} \tag{76}$$

is the dimensionless distance normal to the slider.

For the viscoelastic fluid too it can be verified by substituting the values of u, v and w in equations (9) and (10) that a similarity solution is possible. With the usual definition of R, the cross-flow Reynold's number, one can show that f, g and h satisfy the following BVPs:

$$f''' + R(ff'' - f'^2) + Rk(ff^{\text{iv}} - 2ff''' + f''^2) = A, \tag{77}$$

$$g'' + R(fg' - f'g) + Rk(fg''' - f'g'' + f''g' - f'''g) = 0, \tag{78}$$

$$h'' + Rfh' + Rk(fh''' - 2f'h'' - f''h') = 0, \tag{79}$$

with the boundary conditions

$$\begin{aligned} &f(0)=0, \quad f'(0)=0, \quad f(1)=1. \quad f'(1)=0, \\ &g(0)=1, \quad g(1)=0, \quad h(0)=1, \quad h(1)=0. \end{aligned} \tag{80}$$

The pressure p at any point is given by

$$p(x,z) = p_0 - \tfrac{1}{2}\rho w^2 + \mu\frac{\partial w}{\partial z} - k_0\left[w\frac{\partial^2 w}{\partial z^2} - 2\left(\frac{\partial w}{\partial z}\right)^2\right] + \frac{\rho W^2 x^2 A}{2d^2 R}. \tag{81}$$

The above set of equations, it may be remarked, is a particular case of the set of corresponding equations derived by Bhatt[22] for an elliptical porous slider using a second-order fluid. Bhatt obtained the first-order perturbation solution assuming R small.

4.1. Exact numerical solution

It can be seen that the BVP for f given by equations (77) and (80) is exactly the same as the one given by equations (26) and (27) in Section 3. Its solution has been discussed in detail there. Therefore, we need to consider the solutions of the BVPs for g and h only, which are given by equations (78)–(80)

Note that the differential equations for both g and h are linear, but they have, by now the familiar characteristic of having their order higher than the number of boundary conditions. We can follow the procedure of superimposition given in Section 3.2 to obtain the numerical solutions for g and h. Thus, in order to obtain the solution for g, we write

$$g = g_1 + \beta g_2, \tag{82}$$

where g_1 and g_2 satisfy the IVPs

$$\begin{gathered} g_1'' + R(fg_1' - f'g_1) + Rk(fg_1''' - f'g_1'' + f''g_1 - f'''g_1) = 0, \\ g_1(0) = 1, \qquad g_1'(0) = 0. \end{gathered} \tag{83}$$

and

$$g_2'' + R(fg_2' - f'g_2) + Rk(fg_2''' - f'g_2'' + f''g_2 - f'''g_2) = 0,$$
$$g_2(0) = 0, \qquad g_2'(0) = 1. \tag{84}$$

β in equation (82) can now be identified with $g'(0)$ and is given by the terminal condition

$$\beta = -\frac{g_1(1)}{g_2(1)}. \tag{85}$$

It is worth pointing out here that for a Newtonian fluid ($k=0$) equation (78) can be integrated backward with any missing initial condition for $g'(1)$ because it is a homogeneous differential equation. The values of g can then be normalized by dividing the set of values of g by the value of g obtained at the terminal point $\eta=0$ by numerical integration. This economy, unfortunately, is not available here, as equation (78) can only be integrated forward, at least, by the techniques reported so far in the literature.[9,10] If we follow the discretization scheme given by Ariel[10] then we need to compute the values of g_1 and g_2 at the first integration step by using the Taylor series expansion of g_1 and g_2 up to the second derivative around $\eta=0$. Other than that, the finite difference equations for g_1' and g_2' involve their values at three adjacent mesh points $j-1, j$ and $j+1$, while those for g_1 and g_2 involve the values at the adjacent mesh-points j and $j+1$. One can, therefore, adopt the procedure described in Section 3.1 to compute the values of g_1 and g_2 at each mesh-point. The value of β is determined from equation (85) and, finally, g can be obtained from equation (82). A similar approach is taken to compute the values of h numerically.

Note that the solutions for g and h are restricted to a range of values of k less than a critical value k_c. This is dictated by the corresponding restriction imposed on the solution for f.

4.2. *Perturbation solution for small R*

We seek a perturbation solution for g and h given by

$$g = g_0 + Rg_1 + R^2 g_2 + \cdots$$
$$h = h_0 + Rh_1 + R^2 h_2 + \cdots. \tag{86}$$

Substituting for f from equation (44) and for g and h from equation (86), we get the following BVPs for g and h

$$g_0'' = 0, \qquad h_0'' = 0,$$
$$g_0(0) = 1, \qquad g_0(1) = 0, \qquad h_0(0) = 1, \qquad h_0(1) = 0 \tag{87}$$

and

$$g_i'' + \sum_{j=0}^{i-1} [f_{i-1} g_{i-1-j}' - f_{i-1}' g_{i-1-j} + k(f_{i-1} g_{i-1-j}''' - f_{i-1}' g_{i-1-j}''$$
$$+ f_{i-1}'' g_{i-1-j}' - f_{i-1}''' g_{i-1-j}')] = 0,$$
$$g_i(0) = 0, \qquad g_i(1) = 0 \tag{88}$$
$$h_i'' + \sum_{j=0}^{i-1} [f_{i-1} h_{i-1-j}' + k(f_{i-1} h_{i-1-j}''' - 2f_{i-1}' h_{i-1-j}'' - f_{i-1}'' h_{i-1-j}')] = 0,$$
$$h_i(0) = 0, \qquad h_i(1) = 0 \quad i = 1, 2 \ldots.$$

Equations (87) and (88) can be readily integrated to yield

$$
\begin{aligned}
g(\eta)=1-\eta+R\left[-\frac{9}{20}\eta+\eta^3-\frac{3}{4}\eta^4+\frac{1}{5}\eta^5+3k\eta(1-\eta)\right]\\
+R^2\left[\frac{16}{315}\eta+\frac{8}{105}\eta^3-\frac{383}{1680}\eta^4+\frac{9}{70}\eta^5-\frac{1}{20}\eta^6+\frac{1}{20}\eta^7-\frac{19}{560}\eta^8+\frac{2}{315}\eta^9\right.\\
\left.+k\left(-\frac{103}{70}\eta+\frac{59}{140}\eta^2+\frac{9}{4}\eta^4-\frac{3}{2}\eta^5+\frac{3}{10}\eta^6\right)+9k^2\eta(1-\eta)\right]+O(R^3)
\end{aligned}
\tag{89}
$$

and

$$
\begin{aligned}
h(\eta)=1-\eta+R\left[-\frac{3}{20}\eta+\frac{1}{4}\eta^4-\frac{1}{10}\eta^5+k(\eta-3\eta^2+2\eta^3)\right]\\
+R^2\left[-\frac{2}{525}\eta+\frac{19}{336}\eta^4-\frac{6}{175}\eta^5-\frac{9}{140}\eta^7+\frac{33}{560}\eta^8-\frac{11}{840}\eta^9\right.\\
+k\left(-\frac{1}{70}\eta-\frac{19}{28}\eta^2+\frac{24}{35}\eta^3-\frac{1}{4}\eta^4+\frac{19}{10}\eta^5-\frac{23}{10}\eta^6+\frac{23}{35}\eta^7\right)\\
\left.+k^2\left(\frac{13}{5}\eta+3\eta^2-20\eta^3+24\eta^4-\frac{48}{5}\eta^5\right)\right]+O(R^3).
\end{aligned}
\tag{90}
$$

The expressions for g and h reduce to the corresponding results for a Newtonian fluid ($k=0$) derived by Skalak and Wang.[11] However, for a second-order fluid, the first-order results of Bhatt[22] seem to be in error; his expression for f does not satisfy the boundary condition $f(1)=0$.

4.3. *Asymptotic solution for large R*

For proper asymptotic solutions of g and h, one should bear in mind, that these solutions are only possible for the values of Rk less than a certain quantity, which approaches the value γ defined by (62). This restriction is inherited from the solution for f. Equations (78) and (79) are, therefore, written as

$$g''+R(fg'-f'g)+\alpha(fg'''-f'g''+f''g'-f'''g)=0, \tag{91}$$

$$h''+Rf'+\alpha(fh'''-2f'h''-f''h')=0, \tag{92}$$

where α is given by equation (49).

For outer solution, one writes

$$
\begin{aligned}
g=g_0+\varepsilon g_1+\varepsilon^2 g_2+\cdots\\
h=h_0+\varepsilon h_1+\varepsilon^2 h_2+\cdots
\end{aligned}
\tag{93}
$$

ε being defined by equation (52).

The first two terms of the outer expansion satisfy the BVPs

$$
\begin{aligned}
f_0g_0'-f_0'g_0=0,\quad g_0(1)=0,\\
f_0g_1'+f_1g_0'-f_0'g_1-f_1'g_0=0,\quad g_1(1)=0,\\
f_0h_0'=0,\quad h_0(1)=0,\\
f_0h_1'+f_1h_0'=0,\quad h_1(1)=0.
\end{aligned}
\tag{94}
$$

The only solution of the above system is

$$g_0 = g_1 = 0, \qquad h_0 = h_1 = 0. \tag{95}$$

For the inner solution, we seek the expansions of g and h as under

$$\begin{aligned} g &= G_0(Y) + \varepsilon G_1(Y) + \varepsilon^2 G_2(Y) + \cdots \\ h &= H_0(Y) + \varepsilon H_1(Y) + \varepsilon^2 H_2(Y) + \cdots, \end{aligned} \tag{96}$$

where Y is the stretched variable already defined by equation (58).

The BVPs for G_0 and H_0 are

$$G_0'' + F_0 G_0' - F_0' G_0 + \tfrac{1}{2}\pi\alpha(F_0 G_0''' - F_0' G_0'' + F_0'' G_0' - F_0''' G_0) = 0, \tag{97}$$

$$H_0'' + F_0 H_0' + \tfrac{1}{2}\pi\alpha(F_0 H_0''' - 2F_0' H_0'' - F_0'' H_0') = 0, \tag{98}$$

with the boundary conditions

$$G_0(0) = 1, \qquad G_0(\infty) = 0, \qquad H_0(0) = 1, \qquad H_0(\infty) = 0. \tag{99}$$

If equation (60) is differentiated with respect to Y, it yields

$$F_0^{\text{iv}} + F_0 F_0''' - F_0' F_0'' + \tfrac{1}{2}\pi\alpha(F_0 F_0^{\text{v}} - F_0' F_0^{\text{iv}}) = 0, \tag{100}$$

from which it is easy to see that $G_0 = F_0''$ satisfies equation (97). Hence, the appropriate solution of G_0 satisfying boundary condition (99) is

$$G_0(Y) = \frac{F_0''(Y)}{F_0''(0)}. \tag{101}$$

A similar result holds for Newtonian fluids and this has been demonstrated by Skalak and Wang.[11]

Unfortunately, for a viscoelastic fluid, the solution for H_0 is not as simple as that for a Newtonian fluid, for which it can be expressed in terms of double quadrature. Equation (98) must be integrated numerically marching forward. The technique of integration is similar to the one enunciated in Section 3.3. In Figure 6, the solution curves for H_0 are given for various values of α. Note that for non-zero values of α there are oscillations in H_0, their amplitude increasing with α. This is, indeed, expected, for G_0, the corresponding function along x-axis also has similar oscillations in view of the oscillations in $F_0'(Y)$, and consequently in $F_0''(Y)$.

4.4. Results and discussion

In Figures 7 and 8, g and h, the lateral velocity components along x- and y-axes are plotted for various values of R and k. It can be seen from the figures that in contrast to the plots of f and f', those of g and h are distinguished by oscillations for non-zero values of k and sufficiently large values of R. This behaviour can only be found out by either the exact numerical solution or the asymptotic solution for large R. One may also note from Figure 7 that there is a crucial difference in the nature of g, the lateral velocity along x-axis for small, moderate and large values of R. For small R, g increases with k for all values of η. While for moderate values of R, g decreases with k for all values of η. However, for large values of R, g first decreases with k for smaller values of η, but then as η is increased, the oscillations take place the amplitude of which increases with k.

For h, the lateral velocity along y-axis, a similar behaviour can be seen, except for a small though important detail. We note from Figure 8 that for small values of R, h first increases with k up to certain value of η (which depends on k), but for values of η larger than this value, h actually

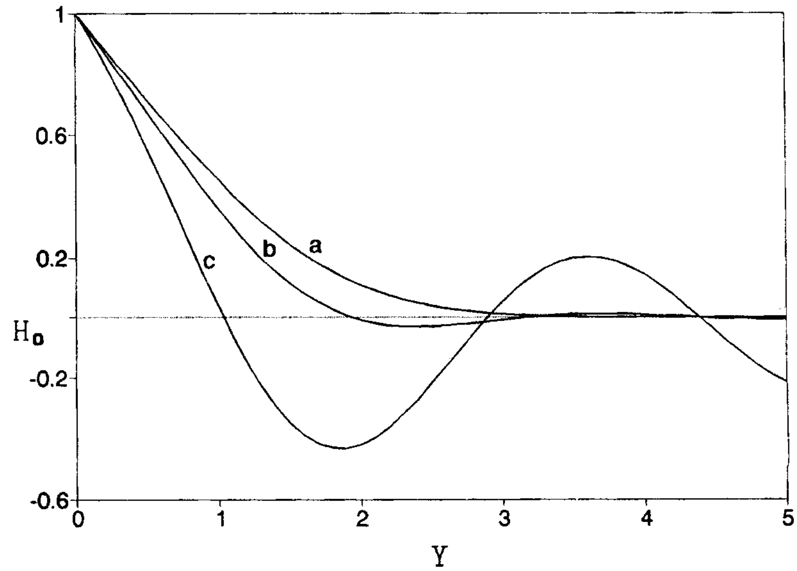

Figure 6. Flow in a porous slider—variation of H_0, the zeroth-order asymptotic solution for h, the lateral velocity along y-direction with Y, for various values of α (=Rk). Curve a: $\alpha=0$, Curve b: $\alpha=0{\cdot}1$, Curve c: $\alpha=0{\cdot}2$

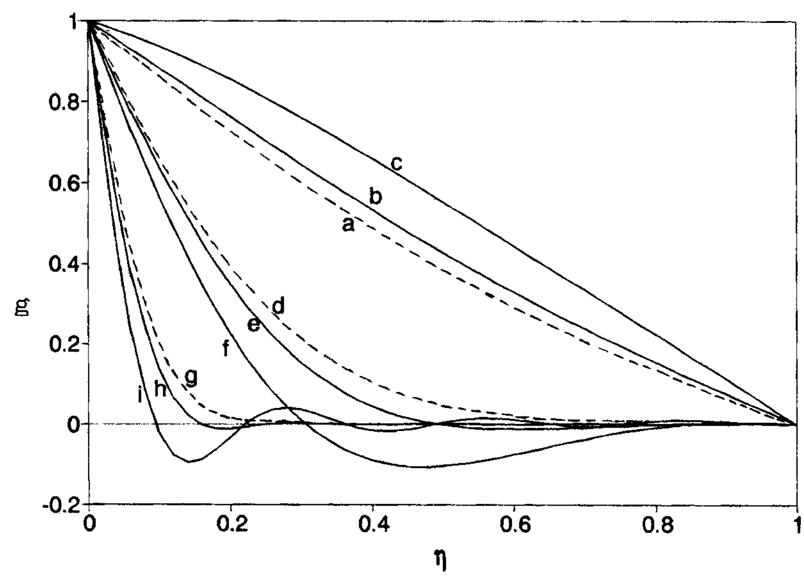

Figure 7. Flow in a porous slider—variation of g, the lateral velocity along x-axis with η for various values of R, the cross-flow Reynold's number, and k, the viscoelastic parameter. (—): the values for a non-Newtonian fluid; (----) the values for a Newtonian fluid. Curve a: $R=1$, $k=0$; Curve b: $R=1$, $k=0{\cdot}1$; Curve c: $R=1$, $k=0{\cdot}2$; Curve d: $R=10$, $k=0$; Curve e: $R=10$, $k=0{\cdot}01$; Curve f: $R=10$, $k=0{\cdot}02$; Curve g: $R=100$, $k=0$; Curve h: $R=100$, $k=0{\cdot}001$; Curve i: $R=100$, $k=0{\cdot}002$

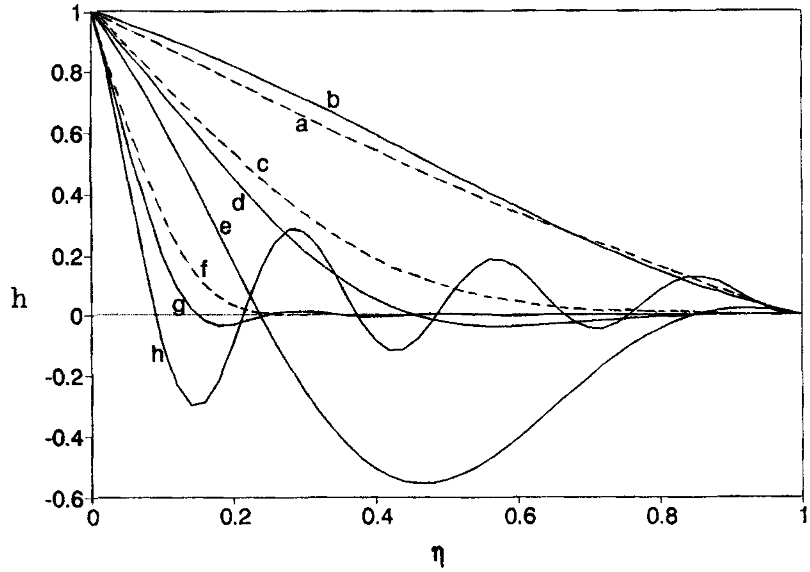

Figure 8. Flow in a porous slider—variation of h, the lateral velocity along y-axis with η for various values of R, the cross-flow Reynold's number, and k, the viscoelastic parameter. (—): the values for a non-Newtonian fluid; (----) the values for a Newtonian fluid. Curve a: $R=1, k=0$; Curve b: $R=1, k=0{\cdot}2$; Curve c: $R=10, k=0$; Curve d: $R=10, k=0{\cdot}01$; Curve e: $R=10, k=0{\cdot}02$; Curve f: $R=100, k=0$; Curve g: $R=100, k=0{\cdot}001$; Curve h: $R=100, k=0{\cdot}002$

decreases with k. This has an important bearing on the value $h'(1)$ in contrast to that of $g'(1)$. For all values of R, $-h'(1)$ decreases with k. However, $-g'(1)$ decreases with k for only moderate to large values of R. For small values of R it actually increases with k.

In Table III, the values of $g'(0)$ and $h'(0)$ are presented for various values of R and k using (i) exact numerical solution, (ii) perturbation solution for small R, and (iii) asymptotic solution for large R. As in the case of flow through a porous channel, the perturbation solution gives acceptable results for values of R up to unity, only for small values of k ($<0{\cdot}2$). The asymptotic solutions given by equation (101) and the numerical solution of equation (98) can be used for values of R exceeding 20–30, *provided* $RK<\gamma$, γ being given by equation (62).

For a porous slider, the important physical quantities are lift L and the drag with components (D_x, D_y). They are given by

$$L=\iint (p-p_a)\,\mathrm{d}\sigma=\frac{\rho^3 W^4 L_1^3 L_2}{12\eta_0^2}\left(-\frac{A}{R^3}\right), \tag{102}$$

$$D_x=\iint \tau_{xz}\Big|_{z=d}\,\mathrm{d}\sigma=\rho U W L_1\, L_2\left[-\frac{1}{R}\,g'(1)-kg''(1)\right], \tag{103}$$

$$D_y=\iint \tau_{yz}\Big|_{z=d}\,\mathrm{d}\sigma=\rho V W L_1\, L_2\left[-\frac{1}{R}\,h'(1)-kh''(1)\right], \tag{104}$$

where p_a is the pressure at the edge of the slider.

As noted above, the behaviour of $-g'(1)$ and $-h'(1)$, in particular, that of the former, depends to a large extent on the values of R for a given value of k. These quantities figure in the expressions for drags D_x and D_y. Therefore, we must make a distinction between the cases $R=O(1)$ and $R\gg 1$.

Table III. Variation of $g'(0)$ and $h'(0)$ with R and k using (i) exact numerical integration, (ii) perturbation solution for small R, and (iii) asymptotic solution for large R

R	k	$g'(0)$		$h'(0)$	
		Exact	Perturbation	Exact	Perturbation
0·2	0	−1·088029	−1·087968	−1·030147	−1·030152
	0·1	−1·030257	−1·030254	−1·009208	−1·009170
	0·2	−0·964666	−0·965340	−0·986014	−0·986107
	0.5	−0.700942	−0.727397	−0.899598	−0.904438
	1·0	0·257879	−0·186825	−0·680271	−0·726724
1	0	−1·405982	−1·399206	−1.153102	−1·153810
	0·1	−1·155383	−1·156349	−1·029846	−1·029238
	0·2	−0·541463	−0·733492	−0·795851	−0·852667
	0·5	−3·660024	1·615079	−0·076074	−0·010952
2	0	−1·744503	−1·696825	−1·309633	−1·315238
	0·1	−1·291448	−1·355397	−0·971497	−1·016952
	0·2	−5·048551	−0·233968	−0·191910	−0·510667
		Exact	Asymptotic	Exact	Asymptotic
20	0	−4·792183	−4·472136	−3·352567	−3·197453
	0·005	−5·272382	−5·092555	−3·585275	−3·461947
	0·01	−6·384905	−6·495494	−3·585874	−4·050210
25	0	−5·329621	−5·084077	−3·732558	−3·574861
	0·004	−5·884728	−5·693648	−4·007301	−3·870575
	0·008	−7·141706	−7·262183	−4·289630	−4·528273
50	0	−7·438635	−7·189971	−5·220342	−5·055617
	0·002	−8·270269	−8·052035	−5·621608	−5·473819
	0·004	−10·334113	−10·270278	−5·831044	−6·403945
100	0	−10·419938	−10·168154	−7·319998	−7·149722
	0·001	−11·625380	−11·387297	−7·892178	−7·741149
	0·002	−14·640878	−14·524367	−8·315064	−9·056546

Also, as pointed out by Wang,[20] the currently available sliders operate at cross-flow Reynold's number less than unity; therefore, such a distinction would indeed be appropriate.

In Figure 9, the normalized values of L, D_x and D_y are plotted against R in the range $0{\cdot}1 \leqslant R \leqslant 1$ for various values of k. It can be seen from the figure that both, the lift L, and the drags D_x and D_y decrease with R for a given value of k, the ratio of lift and drag, represented by the distance between the curves on the log-scale, being larger for smaller values of R. Therefore, the original conclusion of Wang and his co-workers,[11,18–21] namely that, for optimum efficiency, the porous sliders should be operated at small values of R, rather than at moderate values, still remains valid even when the viscoelastic fluid is used.

To see the effect of fluid viscoelasticity on the performance of the slider, we note from Figure 9, that for $R<1$, the value of L decreases with increasing k, keeping R fixed. Also the value of D_y decreases with increasing k for a fixed R, but that of D_x increases as k is increased. Thus, if the viscoelastic fluid is to be used for porous sliders operating at low cross-flow Reynold's number, it is advantageous to move it along y-axis, rather than along x-axis, which is the preferred way for a Newtonian fluid.

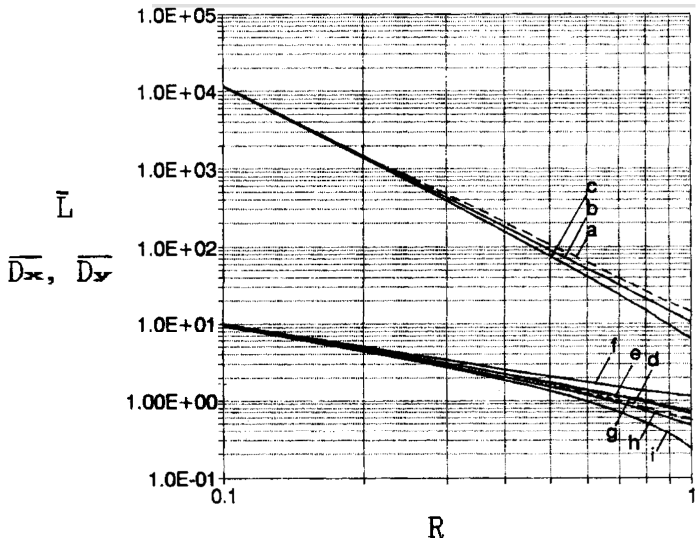

Figure 9. Flow in a porous slider—variation of the normalized lift $\bar{L}(=12\eta_0^2 L/\rho W^4 L_1^3 L_2)$, the normalized drag components $\bar{D}_x\,(=D_x/\rho U W L_1 L_2)$ and $\bar{D}_y(=D_y/\rho V W L_1 L_2)$ with R, the cross-flow Reynold's number, for various values of k, the viscoelastic parameter. (——): the values for a non-Newtonian fluid; (-----): the values for a Newtonian fluid. Curve a: $\bar{L}$ for $k=0$, Curve b: $\bar{L}$ for $k=0{\cdot}1$, Curve c: $\bar{L}$ for $k=0{\cdot}2$, Curve d: $\bar{D}_x$ for $k=0$, Curve e: $\bar{D}_x$ for $k=0{\cdot}1$, Curve f: $\bar{D}_x$ for $k=0{\cdot}2$, Curve g: $\bar{D}_y$ for $k=0$, Curve h: $\bar{D}_y$ for $k=0{\cdot}1$, Curve i: $\bar{D}_y$ for $k=0{\cdot}2$

The situation changes when large values of R are considered. Wang and his co-workers,[11,18–21] for a Newtonian fluid, have also pointed out that the performance becomes progressively better as the value of R is increased beyond a critical value. For this critical value the porous slider's efficiency is minimum. In Figure 10, the normalized values of L, D_x and D_y are plotted for $R \geqslant 1$. For a given value of k, the distance between the curve L on the one hand and the curves D_x and D_y on the other keep on narrowing up to $R=4$, implying a loss of efficiency, but for larger values of R, this distance keeps on widening. This means that the observations of Wang and his co-workers for large values of R still hold for viscoelastic fluid. One can see from Figure 10 that the effect of viscoelasticity is felt most on the drag. The lift decreases with an increase in k only marginally, but the drags in both the directions decrease drastically for values of R near 10 as k is increased. It is remarkable that an increase in the value of R reverses the role played by viscoelasticity on the drag in x-direction; for lower values of R, D_x increases with an increase in the value of k; but, for higher values of R, the opposite is true. Though at present the porous sliders are designed to operate at values of R up to unity, in future, as and when they become available for large values of R, the use of viscoelastic fluids can lead to their much improved performance.

5. FLUID INJECTION THROUGH ONE SIDE OF A VERTICAL CHANNEL

In this section, we consider the flow of Walter's B' fluid injected through one side of a long vertical channel. We assume one wall of the channel to be impermeable and situated in the plane $y=0$, centred at the origin. The fluid is injected through the porous wall $y=d$ with uniform velocity V. Since the gravity effects are taken into account, the fluid flows out of the sides and the bottom of the channel. The dimensions of the channel walls are L_1 and L_2 along x- and z-directions,

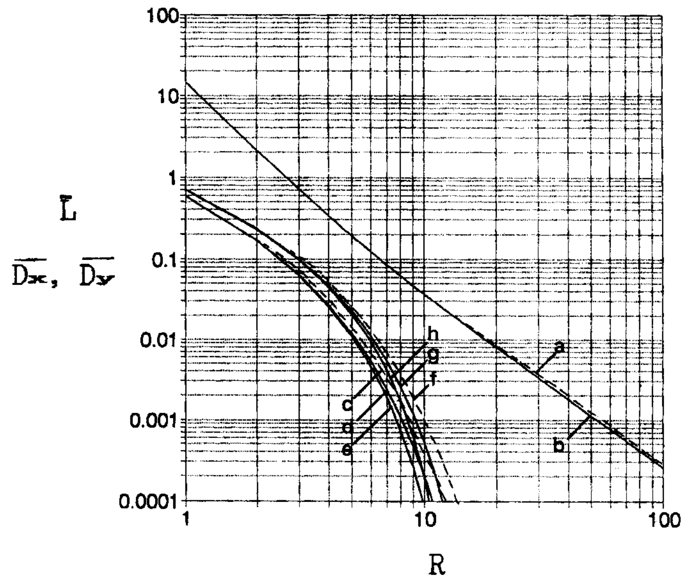

Figure 10. Flow in a porous slider—variation of the normalized lift $\bar{L}(=12\eta_0^2 L/\rho W^4 L_1^3 L_2)$, the normalized drag components $\bar{D}_x$ $(=D_x/\rho U W L_1 L_2)$ and $\bar{D}_y(=D_y/\rho V W L_1 L_2)$ with R, the cross-flow Reynold's number, for various values of k, the viscoelastic parameter. (——): the values for a non-Newtonian fluid; (-----): the values for a Newtonian fluid. Curve a: $\bar{L}$ for $k=0$, Curve b: $\bar{L}$ for $k=0{\cdot}002$, Curve c: $\bar{D}_x$ for $k=0{\cdot}2$, Curve d: $\bar{D}_x$ for $k=0{\cdot}001$, Curve e: $\bar{D}_x$ for $k=0{\cdot}002$, Curve f: $\bar{D}_y$ for $k=0$, Curve g: $\bar{D}_y$ for $k=0{\cdot}001$, Curve h: $\bar{D}_y$ for $k=0{\cdot}002$

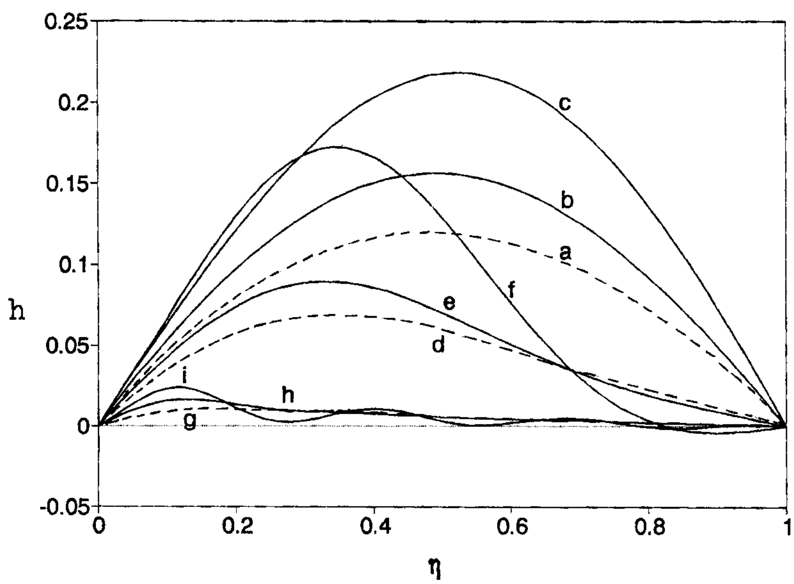

Figure 11. Injection of fluid through the side of a long vertical channel—variation of h, the lateral velocity along vertical direction with η for various values of R, the cross-flow Reynold's number, and k, the viscoelastic parameter. (——) the values for a non-Newtonian fluid (----): the values for a Newtonian fluid. Curve a: $R=1$, $k=0$; Curve b: $R=1$, $k=0{\cdot}1$; Curve c: $R=1$, $k=0{\cdot}2$, Curve c: $R=10$, $k=0$; Curve d: $R=10$, $k=0{\cdot}01$; Curve e: $R=10$, $k=0{\cdot}02$; Curve f: $R=100$, $k=0$; Curve g: $R=100$, $k=0{\cdot}001$; Curve h: $R=100$, $k=0{\cdot}002$.

respectively. It is further assumed that $L_2 \gg L_1 \gg d$, so that the edge effects can be ignored and the isobars are parallel to the z-axis.

For a Newtonian fluid, Wang and Skalak[12] have demonstrated that the Navier–Stokes equations admit a similarity solution, if the velocity components (u, v, w) are chosen as

$$u=\frac{Vx}{d}f'(\eta), \qquad v=-Vf(\eta) \quad \text{and} \quad w=\frac{gd^2\rho}{\eta_0}h(\eta), \tag{105}$$

where

$$\eta=\frac{y}{d} \tag{106}$$

and g is the acceleration due to gravity.

It turns out that the same choice of the velocity components also leads to a similarity solution for a Walter's B' fluid. For the latter fluid, we obtain the following BVPs for f and h:

$$f'''+R(ff''-f'^2)+Rk(ff^{\text{iv}}-2ff'''+f''^2)=A \tag{107}$$

$$h''+Rfh'+1+Rk(fh'''-2f'h''-f''h')=0, \tag{108}$$

with the boundary conditions

$$f(0)=0 \qquad f'(0)=0, \qquad f(1)=1, \qquad f'(1)=0, \qquad h(0)=0, \qquad h(1)=0. \tag{109}$$

Further, p, the pressure at any point is

$$p=p_0-\tfrac{1}{2}\rho v^2+\mu\frac{\partial v}{\partial y}-k_0\left[v\frac{\partial^2 v}{\partial y^2}-2\left(\frac{\partial v}{\partial y}\right)^2\right]+\frac{\rho V^2x^2A}{2d^2R}. \tag{110}$$

As in the problem of porous slider, the BVP for f is exactly the same as for the flow of viscoelastic fluid through a porous channel, and is given by equations (26) and (27). Thus, the BVP for f is fundamental for all the three problems considered in the present paper. The BVP for h (equations (108) and (109)), on the other hand, is similar to the one for h for the problem of porous slider; the difference arising out of the effects of gravity and the stationary nature of the wall $y=0$. In view of these similarities, our discussion in the present section will necessarily be brief.

The exact numerical solution for h can be obtained by proceeding along the lines of Section 4.1. The perturbation solution for small R is given by

$$\begin{aligned}h(\eta)=&\frac{1}{2}\eta(1-\eta)+R\left[-\frac{1}{120}\eta-\frac{1}{8}\eta^4+\frac{1}{5}\eta^5-\frac{1}{15}\eta^6+k\left(\frac{1}{2}\eta+\frac{3}{2}\eta^2-4\eta^3+2\eta^4\right)\right]\\&+R^2\left[-\frac{41}{50400}\eta-\frac{5}{672}\eta^4+\frac{17}{840}\eta^5-\frac{9}{700}\eta^6+\frac{9}{280}\eta^7-\frac{9}{140}\eta^8+\frac{13}{315}\eta^9-\frac{13}{1575}\eta^{10}\right.\\&+k\left(\frac{8}{105}\eta+\frac{5}{56}\eta^2-\frac{17}{42}\eta^3+\frac{73}{280}\eta^4-\frac{17}{20}\eta^5+\frac{11}{5}\eta^6-\frac{64}{35}\eta^7+\frac{16}{35}\eta^8\right)\\&\left.+k^2\left(\frac{13}{10}\eta+\frac{3}{2}\eta^2+8\eta^3-30\eta^4+\frac{144}{5}\eta^5-\frac{48}{5}\eta^6\right)\right]+O(R^3).\end{aligned} \tag{111}$$

For $k=0$, the above solution reduces to the one obtained by Wang and Skalak[12] for a Newtonian fluid.

In Figure 11, h is plotted against η for various values of R and k. Consistent with the result of Skalak and Wang,[12] as R is increased, h decreases for viscoelastic fluid as well. The behaviour of

Table IV. Variation of $h'(0)$ with R and k using (i) exact numerical integration, (ii) perturbation solution for small R

R	k	$h'(0)$	
		Exact	Perturbation
0·2	0	0·498301	0·498301
	0·1	0·509117	0·509126
	0·2	0·520937	0·520990
	0·5	0·561340	0·562825
	1·0	0·623797	0·653348
1	0	0·490901	0·490853
	0·1	0·561760	0·561472
	0·2	0·639153	0·658091
	0·5	0·392773	1·103948
2	0	0·480508	0·480079
	0·1	0·659399	0·662556
	0·2	0·485984	0·949032

h on viscoelasticity depends on the size of R. For smaller values of R, h increases with k for all values of η. The larger values of R cause oscillations in the values of h for viscoelastic fluids. Whereas near $\eta=0$ an increase in the value of k for a given R leads to an increase in the value of h, or simply $h'(0)$, the values of h can become less in certain ranges of values of η as the value of k is increased owing to the oscillations, which become more pronounced for large values of R.

In Table IV, the values of $h'(0)$ are presented using the exact numerical solution and the perturbation solution for small R, for various values of R and k. Once again, it is evident that the perturbation solution, even though obtained without making any assumption on the size of k, gives acceptable results only when both R and k are small ($R<1$ and $k<0{\cdot}2$).

6. CONCLUSIONS

In this paper we have considered primarily the flow of a viscoelastic fluid through a porous channel which has one wall impermeable. The flow is characterized by a BVP in which the order of differential equation exceeds the number of boundary conditions. An exact numerical solution is developed utilizing the algorithm given by the present author.[10] It is found that the solutions for the non-Newtonian fluid are only possible if the value of k, the viscoelastic fluid parameter, is less than a critical value which is dependent on R, the cross-flow Reynold's number. This, therefore, places a limit on the value of Rk below which only the solutions are admissible. Consequently, the solutions reported in literature[2] for viscoelastic fluids for some range of values of R and k appear to be in error. The results of the present paper also cast doubts on other investigations undertaken so far of the flow problems of viscoelastic fluids through the channels and near the disks. These problems are currently under study and the results of the investigations will be reported in future communications.

For the main problem, the solutions are also developed for small R and large R. For the former case, an analytical solution is obtained using the perturbation technique up to the terms $O(R^2)$. Such solutions can be found extensively in the literature for various flow problems of viscoelastic fluids. The results of the present paper demonstrate that these solutions are valid only if the value of k, besides that of R, is also small. On the other hand, the asymptotic solution for large

R exhibits a close relationship with the corresponding solution for Hiemenz flow, and as long as the proper restriction on the value of Rk is taken into account, it produces results that are in reasonable agreement with the exact numerical results.

We have, in addition, also investigated two related problems: (a) fluid dynamics of a long porous slider, and (b) injection of fluid through the side of a long vertical porous channel. For these problems there are additional BVPs with the same characteristics, namely, the order of differential equations exceeds the number of boundary conditions. Exact numerical solutions are obtained for these problems. Once again the perturbation solutions fail to give satisfactory results unless both R and k are small. Hence, we conclude that the perturbation solutions for the flow problems of viscoelastic fluids give acceptable solutions only when both the cross-flow Reynold's number and the viscoelastic fluid parameter are small. For the general case, the exact solutions of the original set of equations must be sought rather than those of the perturbed sets.

REFERENCES

1. D. W. Beard and K. Walters, 'Elastico-viscous boundary-layer flows. I, two dimensional flow near a stagnation point', *Proc. Camb. Phil. Soc.*, **60**, 667–674 (1964).
2. G. M. Shreshta, 'Laminar elastico-viscous, flow through channels with porous walls of different permeability', *Appl. Sci. Res.*, **20**, 289–305 (1969).
3. S. P. Mishra and U. Mohapatra, 'Elasticoviscous flow between a rotating and a stationary disk with uniform suction at the stationary disk', *J. Appl. Phys.*, **48**, 1515–1521 (1977).
4. K. R. Rajagopal and T. Y. Na and A. S. Gupta, 'Flow of viscoelastic fluid over a stretching sheet'. *Rheol. Acta*, **23**, 213–215 (1984).
5. P. D. Verma, P. R. Sharma and P. D. Ariel, 'Applying quasi-linearization to the problem of steady laminar flow of a second grade fluid between two rotating porous disks', *J. Tribology Trans. ASME*, **106**, 448–455 (1984).
6. K. R. Frater, 'On the solution of some boundary-value problems arising in elastico-viscous fluid mechanics', *ZAMP*, **21**, 134–137 (1970).
7. R. W. Serth, 'Solution of a viscoelastic boundary layer equation by orthogonal collocation', *J. Eng. Math.*, **8**, 89–92 (1974).
8. K. Y. K. Ng, 'Solution of Navier–Stokes equations by goal programming', *J. Comput. Phys.*, **39**, 103–111 (1981).
9. I. Teipel, 'Die Raumliche Staupunktstromung fur ein viscoelastisches fluid', *Rheol. Acta*, **25**, 75–79 (1986).
10. P. D. Ariel, 'A hybrid method for computing the flow of visco-elastic fluids', *Int. j. numer. methods fluids*, **14**, 757–774 (1992).
11. F. Skalak and C. Y. Wang, 'Fluid dynamics of a long porous slider', *J. Appl. Mech. Trans. ASME*, **42**, 893–894 (1975).
12. C. Y. Wang and F. Skalak, 'Fluid injection through one side of a long vertical channel', *A.I.Ch.E. J.*, **20**, 603–605 (1974).
13. A. S. Berman, 'Laminar flow in channels with porous walls', *J. Appl. Phys.*, **24**, 1232–1235 (1953).
14. I. Proudman, 'An example of steady laminar flow at large Reynold's number', *J. Fluid Mech.*, **9**, 593–602 (1960).
15. K. Hiemenz, 'Die Grenzschicht in einem in den gleichformingen Flussigkeitsstrom eingetauchten gerade Kreiszylinder', *Dingl. Polytech. J.*, **326**, 321–410 (1911).
16. R. M. Terrill and G. M. Shrestha, 'Laminar flow through parallel and uniformly porous walls of different permeability', *ZAMP*, **16**, 470–482 (1965).
17. H. J. Sneck, 'A survey of gas lubricated porous bearings', *J. Lubrication Technol. Trans. ASME*, **90**, 804–809 (1968).
18. C. Y. Wang, 'Fluid dynamics of the circular porous slider', *J. Appl. Mech. Trans. ASME*, **41**, 343–347 (1974).
19. C. Y. Wang, 'Limitation of the Reynolds equation for porous thrust bearings', *J. Lubrication Technol. Trans. ASME*, **97**, 642–643 (1975).
20. C. Y. Wang, 'The Elliptical porous slider at low cross-flow Reynolds numbers', *J. Lubrication Technol. Trans. ASME*, **100**, 444–446 (1978).
21. L. T. Watson, T. Y. Li and C. Y. Wang, 'Fluid dynamics of the elliptic porous slider', *J. Appl. Mech. Trans. ASME*, **45**, 435–436 (1978).
22. B. S. Bhatt, 'The elliptic porous slider at low cross-flow Reynolds number using a non-Newtonian second-order fluid', *Wear*, **71**, 249–253 (1981).